

Article

A Novel Algorithm for MPPT of an Isolated PV System Using Push Pull Converter with Fuzzy Logic Controller

Tehzeeb-ul Hassan ¹, Rabeh Abbassi ², Housseem Jerbi ³, Kashif Mehmood ^{4,5,*},
Muhammad Faizan Tahir ⁶, Khalid Mehmood Cheema ⁴, Rajvikram Madurai Elavarasan ⁷,
Farman Ali ⁸ and Irfan Ahmad Khan ^{9,*}

¹ Department of Electrical Engineering, Punjab University, Lahore 54000, Pakistan; tehzibulhasan@gmail.com

² Department of Electrical Engineering, College of Engineering, University of Ha'il, Hail 1234, Saudi Arabia; r.abbassi@uoh.edu.sa

³ Department of Industrial Engineering, College of Engineering, University of Ha'il, Hail 1234, Saudi Arabia; h.jerbi@uoh.edu.sa

⁴ School of Electrical Engineering, Southeast University, Nanjing 210000, China; kmcheema@seu.edu.cn

⁵ Department of Electrical Engineering, The University of Lahore, Lahore 54000, Pakistan

⁶ School of Electric Power, South China University of Technology, Guangzhou 510000, China; epfaizantahir_2k7@mail.scut.edu.cn

⁷ Electrical and Automotive Parts Manufacturing Unit, AA Industries, Chennai 600123, India; rajvikram787@gmail.com

⁸ Lahore University of Management Sciences, Lahore 54000, Pakistan; farman.ali@lums.edu.pk

⁹ Marine Engineering Technology Department in a Joint Appointment with Electrical and Computer Engineering, Texas A&M University, Galveston, TX 77553, USA

* Correspondence: kashif_mehmood@seu.edu.cn or kashif.mehmood@ee.uol.edu.pk (K.M.); irfankhan@tamu.edu (I.A.K.)

Received: 22 June 2020; Accepted: 30 July 2020; Published: 3 August 2020



Abstract: Photovoltaic (PV) is a highly promising energy source because of its environment friendly property. However, there is an uncertainty present in the modeling of PV modules owing to varying irradiance and temperature. To solve such uncertainty, the fuzzy logic control-based intelligent maximum power point tracking (MPPT) method is observed to be more suitable as compared with conventional algorithms in PV systems. In this paper, an isolated PV system using a push pull converter with the fuzzy logic-based MPPT algorithm is presented. The proposed methodology optimizes the output power of PV modules and achieves isolation with high DC gain. The DC gain is inverted into a single phase AC through a closed loop fuzzy logic inverter with a low pass filter to reduce the total harmonic distortion (THD). Dynamic simulations are developed in Matlab/Simulink by MathWorks under linear loads. The results show that the fuzzy logic algorithms of the proposed system efficiently track the MPPT and present reduced THD.

Keywords: fuzzy logic control; maximum power point tracking; photovoltaic; push pull converter; off-grid voltage source inverter

1. Introduction

Energy is the need of the modern world, but its conventional sources are depleting with each passing day, which includes thermal, nuclear, and natural gas [1–3]. These sources are insufficient and not environment friendly [4,5]. Therefore, it is becoming imperative to find alternate sources of energy that can meet the requirements of energy in the future and should be environmentally friendly [6]. High prices of electrical energy from thermal power plants and intermittency of renewable

energy sources [2] move extra emphasis towards hydro-thermal scheduling [7]. Additionally, owing to the continuous diminishing of conventional sources [1,2], the active power generation and the control and compensation of reactive power are becoming the focus for the economic dispatch [8–12], and researchers have also found the way to optimally generate, shed, and forecast the electrical power [13–15]. Recently, solar energy has become one of the free, clean, and reliable sources of energy [3,16].

Neeraj et al. employ hybrid neural network and fuzzy-logic control for maximum power point tracking (MPPT) of photovoltaic (PV) [17], while Gul et al. use a fuzzy controller that depends on a distinct combination of inputs and outputs to track MPPT [18]. Ref. [19], ant colony optimization (ACO) algorithm with MPPT is used in case of the hybrid PV-wind system to produce power for rural areas. Moreover, an advanced MPPT method considering temperature variability for a PV system to attain maximum tracking performance is designed by [20]. Therefore, with the passage of time, various MPPT techniques such as incremental conductance (IC), perturb and observe (P&O), and artificial neural networks (ANN) are developed to ensure maximum gain from solar modules [21–23]. Furthermore, in Ref. [24], the center of inertia technique is used to evaluate the performance of an electronic inverter-based PV power system. However, these techniques have shortcomings including an inability to track continuous power and oscillations near the maximum point. Furthermore, conventional techniques are not able to detect the maximum power point accurately when weather conditions change rapidly [25] and computational time is relatively long to calculate the maximum power point. Usually, single switch buck-boost converters are used with these conventional techniques [26]. These converters do not provide the isolation between input and output sides and a high voltage conversion ratio. From the system point of view and utilization of AC loads, the conventional converters produce DC voltages from the PV panels and then invert it into AC through the open loop inverters. These inverters present high total harmonic distortion (THD) [27–30]. Therefore, an active, computationally fast, resilient, and efficient MPPT algorithm is required.

In this paper, a fuzzy logic controller is employed for MPPT to overcome the aforementioned shortcomings by tracking the maximum power point (MPP) in real time. Fuzzy logic based control offers an advantage in that it does not oscillate near the MPP [31,32]. This kind of control is unique for push pull current-fed boost converters where the high frequency transformer is used to provide the galvanic isolation between the input and output side along with a high conversion ratio [33,34]. DC voltage is inverted to AC through a voltage source inverter (VSI) with a fuzzy logic closed loop controller, which improves the power quality of the AC voltage and provides very low THD. In this work, 5% THD is considered, which is tolerable according to the Institute of Electrical and Electronics Engineers (IEEE) standard [35].

The proposed work covers many of the shortcomings mentioned in the introduction section. However, to distinguish the proposed research from the previously published literature, the main contributions of this proposed work are summarized as follows:

1. Design of fuzzy logic based MPPT, which can track the continuous power without oscillations and noise near the maximum point.
2. Implementation of a push pull current-fed boost chopper in which high frequency transformer is used to provide the galvanic isolation between input and output, along with a high conversion ratio.
3. Implementation of a voltage source inverter (VSI) with a fuzzy logic closed loop controller, which improves the power quality of the AC voltage and provides very low THD.
4. Applications of two fuzzy logic controllers (FLCs) are employed in the proposed system and each has its unique fuzzy rule. The first one tracks the MPPT, and the second is used in VSI with a proper designed low pass filter to reduce the THD value.

Furthermore, a comparative section is added at the end, which is based on the literature on the fuzzy logic principle. The comparison includes the methodology used with fuzzy logic, implementation

complexity, generalization in terms of symmetrical and asymmetrical membership function, inputs to the membership functions, hardware implementation, noise and oscillations near MPP, THD analysis, and the proper filter design. This comparative analysis also distinguishes the proposed research from the previously published literature. As a result, the proposed work has advantages in term of simple, accurate, and faster convergence to the operating point with minimum noise and THD levels.

This paper is organized as follows. An equivalent circuit for an individual PV cell based on a single diode model is presented in Section 2 that serves as a basis for MPPT and defines the proposed methodology. The push pull converter and its design aspects are explained in Section 3, while the fuzzy logic based MPPT algorithm is described in Section 4. Furthermore, the push pull converter, VSI, and low pass filter design are explained in Section 4. Simulation results and discussions are in Section 5 and, finally, the conclusions are drawn in Section 6.

2. Proposed Work Methodology

Before discussing the proposed work topology and fuzzy logic control, it is important to elaborate on the equivalent solar circuit.

2.1. Solar Cell Equivalent Circuit

The equivalent circuit of the solar cell is presented in Figure 1 and indicates a current source is connected with parallel diode. Here, R_{se} is a series resistance, R_p is connected in parallel, while R_L is the load resistance. The reverse saturation current of the diode is I_s . The resistance R_p is very high compared with R_{se} . The diode anode current and V_{PV} can be obtained as [36] by applying Kirchhoff current law (KCL) to the solar cell equivalent circuit:

$$I_{Source} - I_d - \frac{V_d}{R_p} - I_{pv} = 0 \quad (1)$$

$$I_d = I_s (e^{\frac{qV_d}{NKT}} - 1) \quad (2)$$

$$V_{PV} = V_d - R_{se}I_{PV} \quad (3)$$

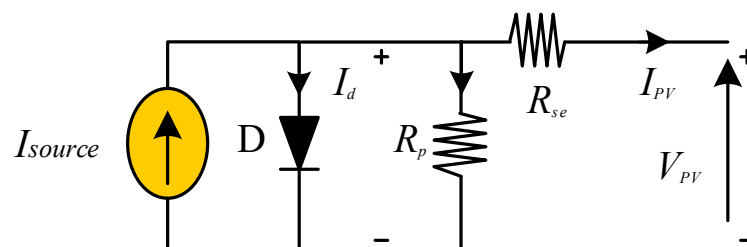


Figure 1. Equivalent circuit of practical single diode model solar cell.

2.2. Proposed Topology

An isolated photovoltaic system is designed for a 500 W solar panel with a fuzzy logic MPPT algorithm. Fuzzy logic closed loop voltage source inverter and low pass filter are employed. Figure 2 shows the proposed system components. Both the voltage and current of the solar PV array are measured to calculate the power. On the basis of the present and previous values of power and current, error and change in error are computed for the fuzzy logic controller that gives the fuzzy rules. On the basis of these fuzzy rules, the fuzzy logic controller sets the duty ratio for pulse width modulation (PWM), 40 kHz triangular wave is compared with the fuzzy logic controller output. The PWM generator produces the switching signal for push pull boost converter switches (which are insulated-gate bipolar transistors (IGBTs)). The push pull boost converter boosts the 60 V DC to 340 V DC. Then, the DC voltages are inverted into 220 V AC through voltage source inverter (VSI). The low

pass filter removes the high frequency harmonic content. The switching of VSI is performed through the unipolar sinusoidal pulse width modulation (USPWM) generator and the unipolar switching technique is employed to mitigate the low order harmonic contents.

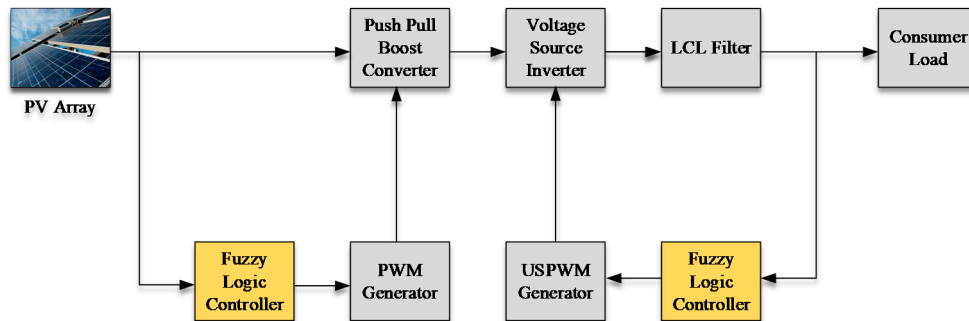


Figure 2. Block diagram of the proposed methodology. USPWM, unipolar sinusoidal pulse width modulation; PV, photovoltaic.

2.3. Fuzzy Logic Control

In the fuzzy logic MPPT algorithm, voltage and current at each instant k are sensed to calculate the active power [31]. The active power is then compared with the power at last instant $k - 1$ to obtain the change in power ($\Delta P(k)$). Similarly, the current at instant k is compared with the current at instant $k - 1$ to achieve the current error ($\Delta I(k)$). Afterwards, the power error is divided by the current error to achieve the error (e), which is compared with the previous error to calculate the change in error ($\Delta e(k)$) as in Equations (4) and (5), respectively. In this way, error $e(k)$ and $\Delta e(k)$ become the crisp inputs of the fuzzy logic controllers. The flow chart for fuzzy logic MPPT is shown in Figure 3.

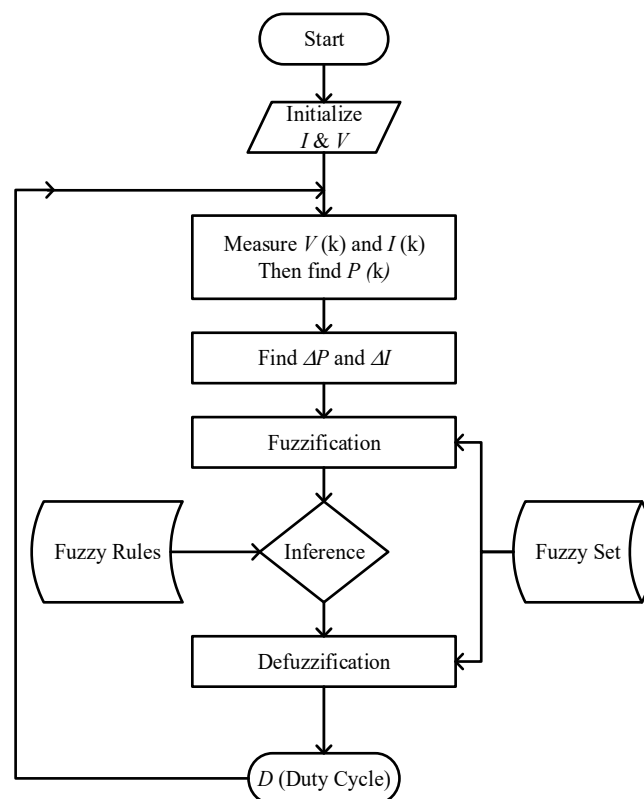


Figure 3. Fuzzy logic maximum power point tracking (MPPT) flow chart.

In this work, Mamdani inference technique, A-type membership functions, and 49-element rule base were used for the fuzzy logic control because of the fact that Mamdani inference technique is efficient and straightforward in defining the fuzzy output sets and is more popular among researchers than other inference techniques [37]. The A-type or triangular type membership function is used because it has fewer complexities when splitting values (low, med, and high (Membership Function) MF) comparing other membership functions. Moreover, it was observed that the triangle membership function gives the faster response and less overshoot than others [38]. The 49-element rule base was employed because it exhibits good performance [39,40].

$$e(k) = \frac{\Delta P(k)}{\Delta I(k)} = \frac{P(k) - P(k-1)}{I(k) - I(k-1)} \quad (4)$$

$$\Delta e(k) = e(k) - e(k-1) \quad (5)$$

Generally, a fuzzy logic controller consist of three components: (i) fuzzifier, (ii) inference, and (iii) defuzzifier [41]. Each component is individually described below.

2.3.1. Fuzzifier

This component of the fuzzy logic controller receives the data from the input and analyzes them according to the user user-defined chart called membership function. Fuzzifier receives the data in the non-linear form and assigns them grade from 0 to 1. Membership functions have different shapes. These shapes depend on the type of data, and but the common shapes are S, π , A, and Z [30]. 'A' shape has been used in this work for fuzzification operation.

2.3.2. Interference

The inference system consists of a fuzzy rule plays an important role in representing the expert control or modeling knowledge between the input and output side. In the literature, different techniques are used in the inference system. Mamdani inference technique with the fuzzy rule is employed in this work. If-then else statements are used in the system for fuzzy inference [42]. For example, we consider a simple two-input one-output example that has three fuzzy rules.

Rule (1) IF X is A_2 OR Y is B_1 Then Z is C_1

Rule (2) IF X is A_2 AND Y is B_2 Then Z is C_3

Rule (3) IF X is A_1 Then Z is C_3

The fuzzy logic membership functions designer, fuzzy logic rule editor, fuzzy logic rules, fuzzy logic member ship function input error, change in error, and membership function output are shown below in Figures 4–7.

The following are the fuzzy rules in Table 1, which are used for desired MPP of push pull converter PWM.

Table 1. Fuzzy logic rules for the push pull converter. NB, negative big; NM, negative medium; NS, negative small; ZE, zero; PS, positive small; PM, positive medium; PB, positive big.

Input	E							
	NB	NM	NS	ZE	PS	PM	PB	
ΔE	NB	ZE	ZE	ZE	NB	NB	NB	NM
	NM	ZE	ZE	ZE	NS	NM	NM	NM
	NS	NS	ZE	ZE	ZE	NS	NS	NS
	ZE	NM	NS	ZE	ZE	ZE	PS	PM
	PS	PS	PM	PM	PS	ZE	ZE	ZE
	PM	PM	PM	PM	ZE	ZE	ZE	ZE
	PB	PB	PB	PB	ZE	ZE	ZE	ZE

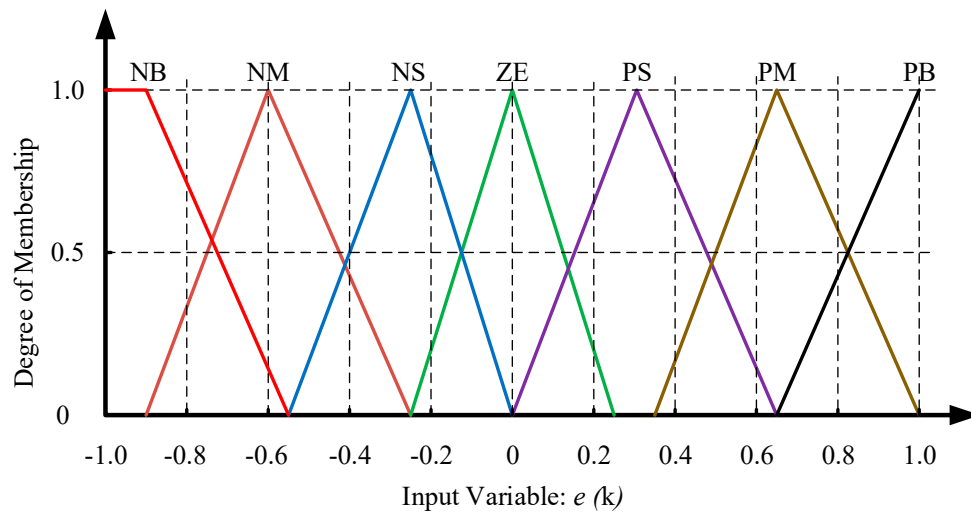


Figure 4. Membership function input error. NB, negative big; NM, negative medium; NS, negative small; ZE, zero; PS, positive small; PM, positive medium; PB, positive big.

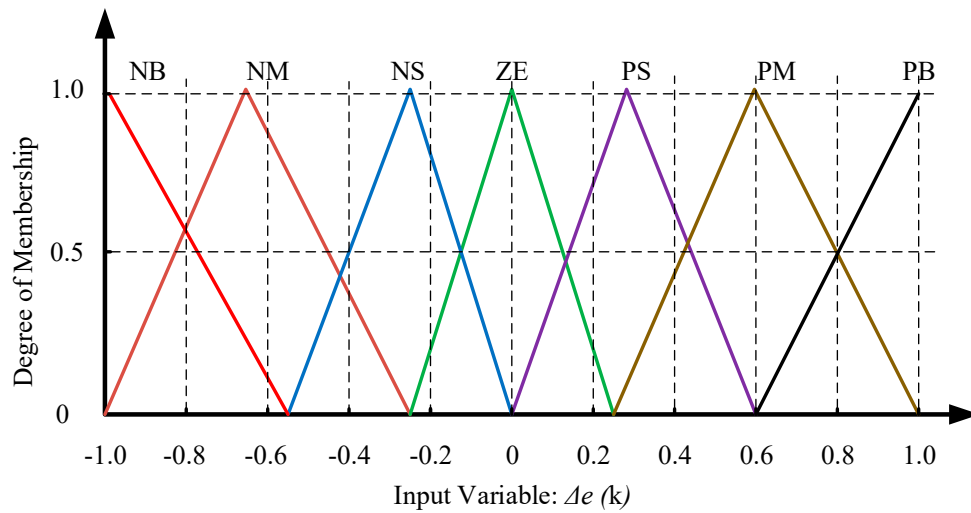


Figure 5. Membership function change in error.

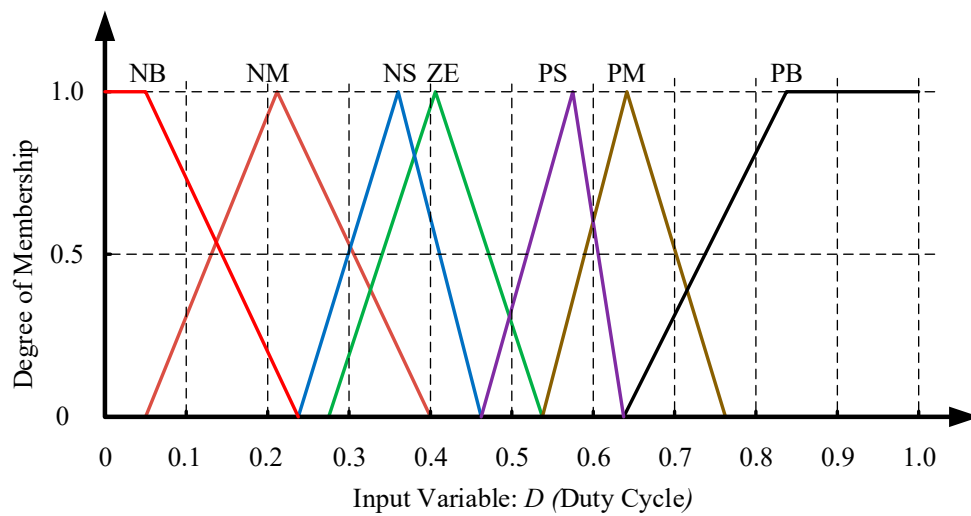


Figure 6. Membership function output.

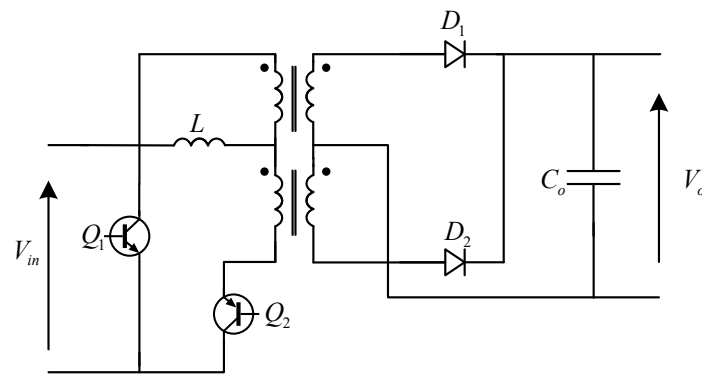


Figure 7. Circuit diagram for the current fed push pull boost converter.

2.3.3. Defuzzification

In the defuzzification process, fuzzy logic controllers use the fuzzy rules to obtain the output value. This output value of the fuzzy logic controller depends upon the method of defuzzification. Hence, it is the gained value of a fuzzy logic controller with respect to the label value in the fuzzy logic membership function. Seven fuzzy membership functions were used in this research, as enlisted in Table 1. These seven functions are negative big (NB), negative medium (NM), negative small (NS), zero (ZE), positive small (PS), positive medium (PM), and positive big (PB). During the defuzzification, the FLC converts the fuzzy logic value into a data value. Numerous methods are available for the defuzzification process such as the average weight (AW) method, center of gravity (COG), mean of maximum (MOM), and smallest of maximum (SOM) [30]. The COG method is used for MPPT in which all fuzzy values are converged at one point [26]. The fuzzy logic rules are used in the push pull boost converter design for MPPT, which is given in Table 1 [42].

3. Push Pull Converter and Its Design Aspects

The push pull converter consists of a centrally tapped transformer, two push pull switches Q_1 and Q_2 , series inductor L , two rectifier diodes D_1 and D_2 , and a parallel capacitor C_0 , as shown in Figure 7. Push pull converter can operate in four states. By applying PWM, the designed inductor and specifications of load ensure that the converter always operates in the continuous conduction mode (CCM) [36,42].

A designed current fed DC–DC push pull boost converter is shown in Figure 7 and its operating characteristics are given in Table 2.

Table 2. Design parameters of the push pull converter. PWM, pulse width modulation.

Parameters	Values
Power	500 W
Input voltage	60 V
Output voltage	340 V
Turn ratio (n)	1:6
Switching frequency	40 kHz
Duty cycle	0.0523
Inductor	518 μ H
Output capacitor	100 μ F
Input Inductor current	9.38 A
PWM switching frequency	10 KHz
Input DC voltage	340 V
Output voltage	V rms
Resistive load	100 Ω

This circuit consists of a center tap transformer, two push pull switches Q_1 and Q_2 , series inductor L , two rectifier diodes D_1 and D_2 , and a parallel capacitor with the output load.

The turn ratio of the transformer is calculated as follows:

$$n = \frac{2V_o(1-D)}{V_{in}} \quad (6)$$

The switches' on and off time are selected as follows:

$$t_{on} = \frac{T}{2} - (D - \frac{1}{2}) = (1-D)T \quad (7)$$

$$t_{off} = (D - \frac{1}{2})T \quad (8)$$

When both switches are in an off state, the voltage across these switches is double. This voltage stress is compensated by selecting a transformer tapping voltage as follows:

$$V_o \cong 1.05 \times V_{in,max} \quad (9)$$

During the dead time, when both switches are in the off position, the inductor increases in a linear mode of operation.

$$V_{in} = \frac{2L\Delta I}{t_{off}} \quad (10)$$

When only one switch is on, the energy is transferred to the secondary side of the transformer, then

$$V_o = V_{in} + \frac{2L\Delta I}{t_{on}} \quad (11)$$

Hence,

$$V_o = V_{in} + \frac{V_{in} \times t_{off}}{t_{on}} = V_{in} \times \frac{1}{2(1-D)} \quad (12)$$

The input current of the inductor with efficiency η is given by the following:

$$I_i = \frac{p_o}{\eta \times V_d} \quad (13)$$

The inductor size is selected carefully, a very value inductor may cause the converter to operate in the discontinuous mode and very high-value inductor may cause an increase in the size and weight of the converter.

$$\Delta I = xI_i \quad (14)$$

where $0.05 \leq x \leq 0.3$ for optimal operation.

$$V_{in} = V_o \times 2(1-D) = \frac{2L\Delta I}{t_{off}} \quad (15)$$

Rearranging the equation

$$L\Delta I = V_o \times 2(1-D) \times \left(D - \frac{1}{2}\right)T \quad (16)$$

Or

$$(\Delta I)_{max} = \frac{V_{ct}}{16Lf_s} \quad (17)$$

The proposed converter operates in CCM; therefore, minimum inductance is required at the output side, which is calculated as represented in Equation (18).

$$L = \frac{V_o}{16 \times f_s (\Delta I)_{\max}} \quad (18)$$

To operate the converter in CCM, the value of the output side capacitor is calculated as shown in Equation (19).

$$C_0 = \frac{P_o(2D-1)}{4V_r \times V_o^2 \times f_s} \quad (19)$$

where V_r is DC ripple voltage, which is 3% allowable.

The proposed converter topology offers the benefit of isolation between the input and output side, maximum efficiency, constant input current, high voltage conversion, the minimum number of switches, simplicity of configuration, and thus low conduction losses. Furthermore, there is no need for a filter capacitor at the input side that makes the system simple and compact [34].

4. VSI and Low Pass Filter Design

In the proposed system, a single-phase full bridge inverter is used to feed the consumer load, which inverts the 340 V DC into 220 V AC at 50 Hz frequency. The unipolar sinusoidal pulse width modulation (USPWM) technique is used to turn on/off the inverter switches. This technique reduces THD and power losses during switching [26]. In USPWM, two control signals are used: a sinusoidal wave and its 180° out of phase version at 50 Hz. These control signals are compared with high frequency triangular carrier signal of 10 kHz. Control signal 1 is compared with the carrier signal, resulting in a logic signal that generates the output voltage between 0 and $+V_{dc}$. Control signal 2 is compared with the carrier signal, resulting in a logic signal that produces the output voltage between 0 and $+V_{dc}$. In every inverter, a filter is necessary for improving power quality. Therefore, a low pass filter is used for smoothing the output current from VSI. The LCL filter is shown in Figure 8.

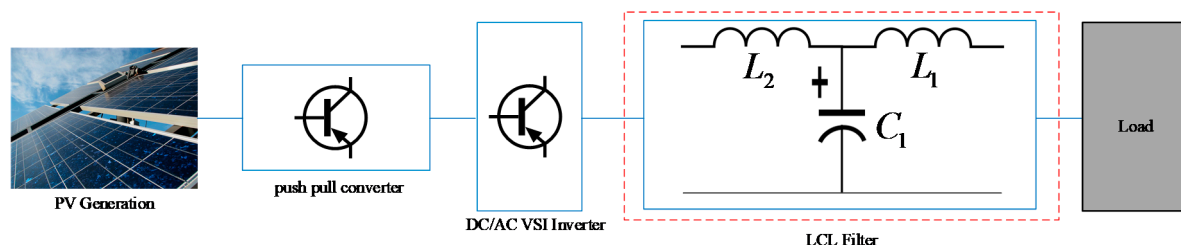


Figure 8. Application of LCL filter in PV system.

The components of the filter are obtained as represented in Equations (20)–(25).

The filter value refers to base impedance

$$Z_b = \frac{E n^2}{P_n} = \frac{V_0^2}{P_n} \quad (20)$$

where Z_b is the base impedance and V_0 and P_n are the output voltage and power of the inverter, respectively. The maximum power variation is considered as 5% and the base impedance is adjusted as computed in Equation (21):

$$C_f = 0.05 C_b \quad (21)$$

where L_1 is inductance on inverter side. For 10% ripple, L_1 is calculated by considering the rated current of the inductor.

$$\Delta I_{L\max} = 0.1 I_{\max} \quad (22)$$

Further, I_{\max} is calculated as shown in Equation (23):

$$I_{\max} = \frac{P_n}{V_o} \quad (23)$$

L_1 is calculated as represented in Equation (24):

$$L_1 = \frac{V_{dc}}{16 f_s \Delta I_{L\max}} \quad (24)$$

where f_s is switching frequency and L_2 is calculated as follows:

$$L_2 = \frac{\sqrt{\frac{1}{K_a^2} + 1}}{C_f \omega_s^2} \quad (25)$$

where K_a is the attenuation factor and is taken as $K_a = 0.2$, while $\omega_s = 2\pi f_s$ is angular switching frequency [41,43].

For LCL filter, derived parameters are $L_1 = 9.3$ mH, $L_2 = 37.5$ mH, and $C = 1.6$ μ F with the unity power factor. The LCL filter designing algorithm is shown in Figure 9. After the filtration, (root mean square) RMS output voltages are sensed for the fuzzy logic controller input. The output of the controller is compared with the sinusoidal AC voltages at the fundamental frequency, and then PWM set the duty of VSI.

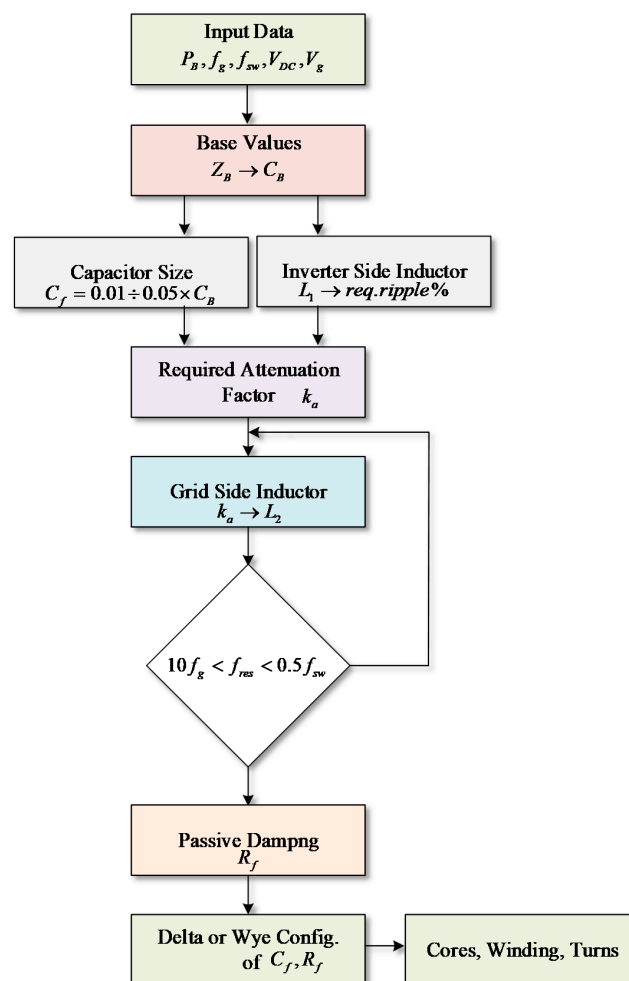


Figure 9. LCL filter design algorithm.

The fuzzy logic structure of VSI is the same as the MPP push pull converter; however, the fuzzy rules used in FLC of VSI are listed in Table 3.

Table 3. Fuzzy logic rules for the voltage source inverter (VSI).

Input	E							
	NB	NM	NS	ZE	PS	PM	PB	
ΔE	NB	NB	NB	NB	NB	NM	NS	ZE
	NM	NB	NB	NB	NM	NS	ZE	PS
	NS	NB	NB	NM	NS	ZE	PS	PM
	ZE	NB	NM	NS	ZE	PS	PM	PB
	PS	NM	NS	ZE	PS	PM	PB	PB
	PM	NS	ZE	PS	PM	PB	PB	PB
	PB	ZE	PS	PM	PB	PB	PB	PB

5. Results and Discussion

The proposed isolated photovoltaic system with a fuzzy logic controller, the current fed push pull DC–DC boost converter, is presented here. The DC–DC boost converter operates in continuous conduction mode, and the voltage source inverter with fuzzy logic closed loop and low pass filter are simulated in Matlab/Simulink. The parameters of the employed PV array (Canadian solar CS5P 250-M) are given in Table 4. The performance of the developed system is tested at different irradiance intensity at 25 °C and a linear load of 200 Ω, as shown in Figure 10. Voltage and current are sensed to calculate the power.

Table 4. Parameters of photovoltaic (PV) array.

PV Array	Parameters
No. of Cells and Connections	96
Open Circuit Voltage	59.4 V
Maximum Power Voltage	48.7 V
Short Circuit Current	5.49 A
Maximum Power Current	5.14 A
Maximum Power	250.318 W
Diode saturation current	2.9177×10^{-11}
Diode ideality factor	0.93246
Shunt resistance	428.442 Ohm

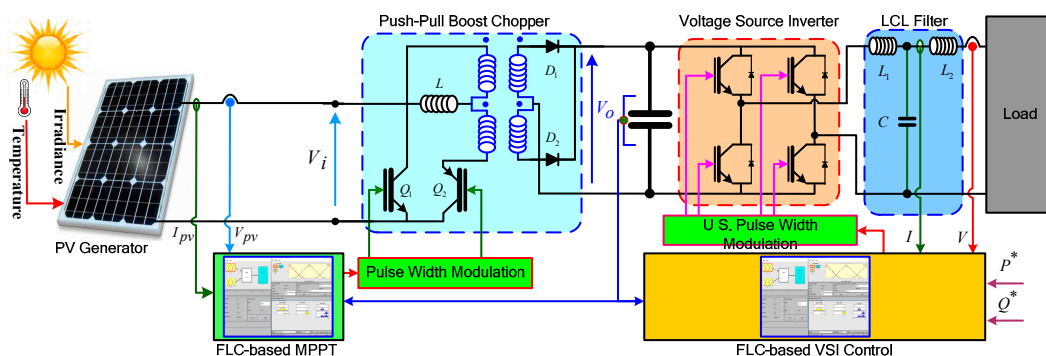


Figure 10. Schematic of the proposed control architecture of the studied system. VSI, voltage source inverter; FLC, fuzzy logic controller.

In the first case, the system is simulated at a constant temperature of 25 °C and constant irradiance 1000 W/m². It tracks the maximum power 250 W in a very small amount of time, approximately 0.005 s, as shown in Figure 11.

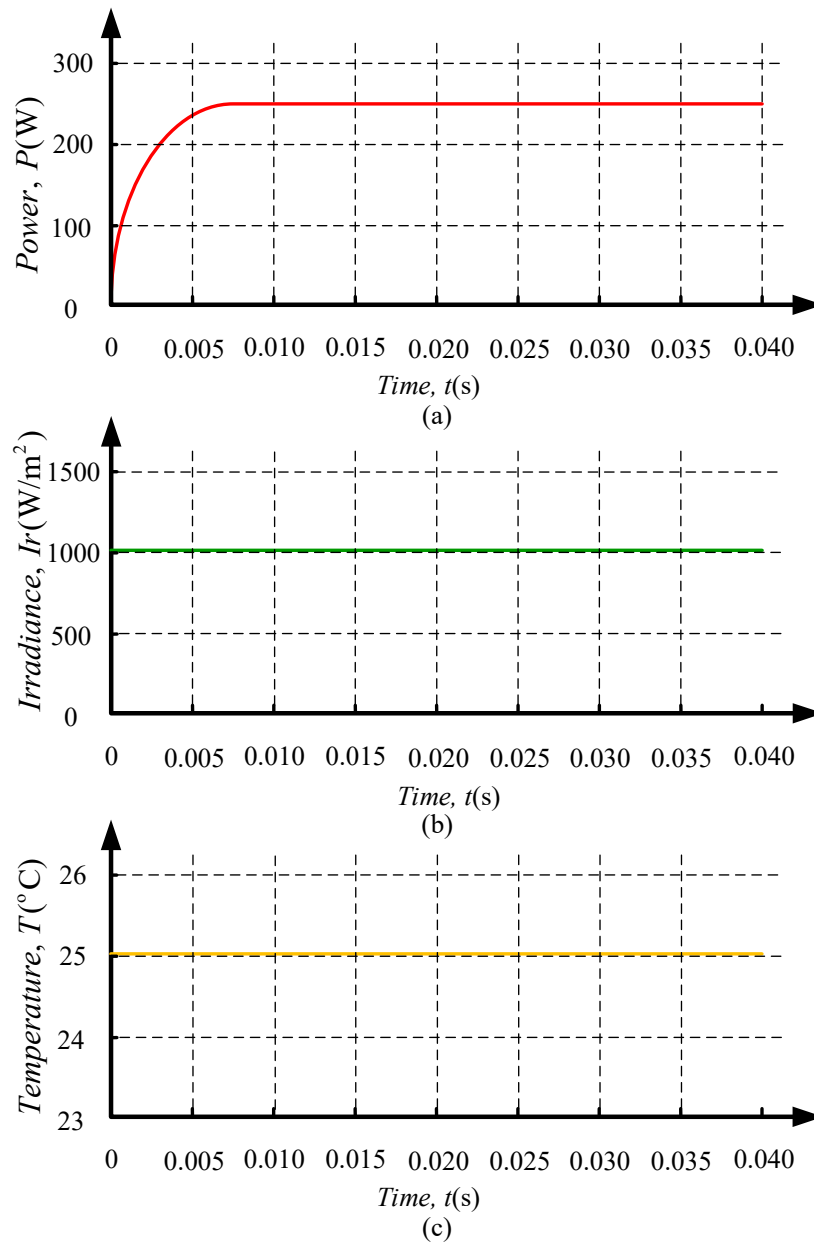


Figure 11. Output: (a) Power versus time at; (b) constant irradiance; (c) constant temperature.

In the second case, the system is simulated for various irradiance levels as follows: 800 W/m² for 0.015 s, 600 W/m² for 0.03 s, and 1000 W/m² for the rest of the time. In this scenario, it again tracks the maximum power point within the same designed spam of time (0.005 s) and gives the power of 200 W, 150 W, and 250 W, respectively, as shown in Figure 12. This power is tracked through the fuzzy logic controller, where fuzzy rules are employed as given in Table 1.

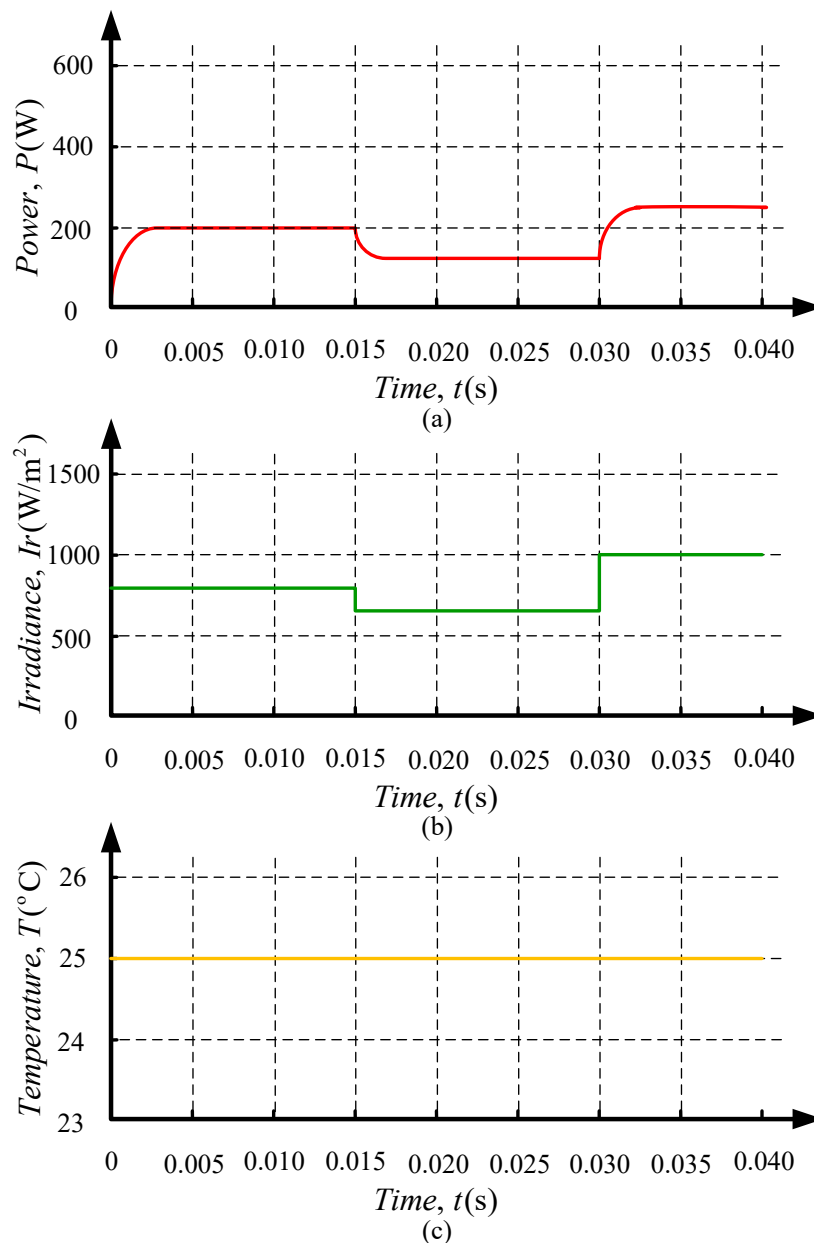


Figure 12. Output: (a) Power versus time at; (b) different irradiance and; (c) constant temperature.

On the basis of the designed fuzzy rules, the fuzzy logic controllers generate the fuzzy logic PWM and decide what would be the duty ratio of the push pull boost converter switches shown in Figure 13a. The push pull boost converter operates in four states. In state 1, when the switch Q_1 is on, then the inductor would discharge, and output voltage would be positive. In state 2, switches Q_1 and Q_2 are ON simultaneously. During state 2, the inductor is charged, as shown in Figure 13c, that is, 4.3 A current flows, and the output voltage would be zero because the flux generated in both windings cancels each other out. In this state, the output capacitor provides the voltage to the load, which means that the capacitor would be discharged. In state 3, when the switch Q_2 is ON, then the voltage would be negative. Similarly, in state 4, both switches are ON simultaneously for zero output voltages, as shown in Figure 13b, that is, modified sine wave voltages, which are converted into 340 V DC through the rectifier diodes D_1 and D_2 , as shown in Figure 13d.

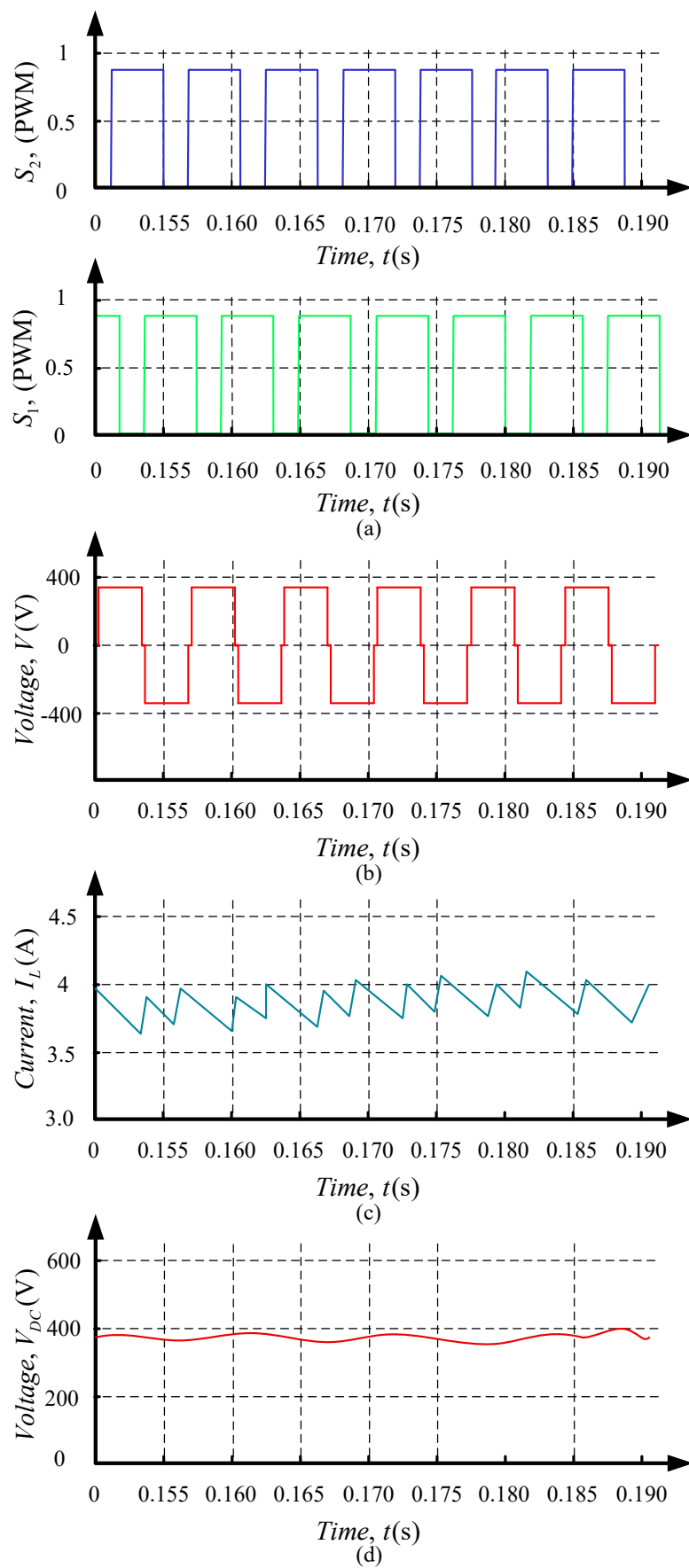


Figure 13. Output: (a) Fuzzy logic PWM; (b) transformer output; (c) inductor current; (d) DC output voltage.

The DC voltages are inverted into 220 V AC through the VSI. These voltages are sensed through the voltage sensor and compared with the sinusoidal AC voltages; error and change in error are calculated for fuzzy FLC. This controller generates the reference signal for the PWM generator, which operates the inverter switches and is operated according to the fuzzy logic controller. The PWM of the inverter is shown in Figure 14a. FLC generates the reference signal by using the fuzzy rules of Table 3, settled down by removing the lower order harmonic content in AC voltages. However, these voltages still have the higher-order harmonic content shown in Figure 14b. The higher-order harmonic contents are removed through the low pass filter. The output voltages and current of inverter after removing the higher-order harmonic content are shown in Figure 15, where Figure 15a presents the AC voltages and Figure 15b shows the AC current, which is 1.5 A.

To check the quality of output voltages and current, the fast Fourier transform (FFT) analysis is also carried out and obtained THD are shown in Figures 16 and 17. The FFT analysis of the proposed algorithm provides only 1.41% THD for output voltage and current at 50 Hz.

To prove the validity of the conducted research, a comparison between the results of the fuzzy logic-based MPPT algorithm is compared with P&O and incremental conductance algorithms available in the literature, in the time domain function at irradiance 1000 W/m^2 and at $25 \text{ }^\circ\text{C}$, as listed in Table 5.

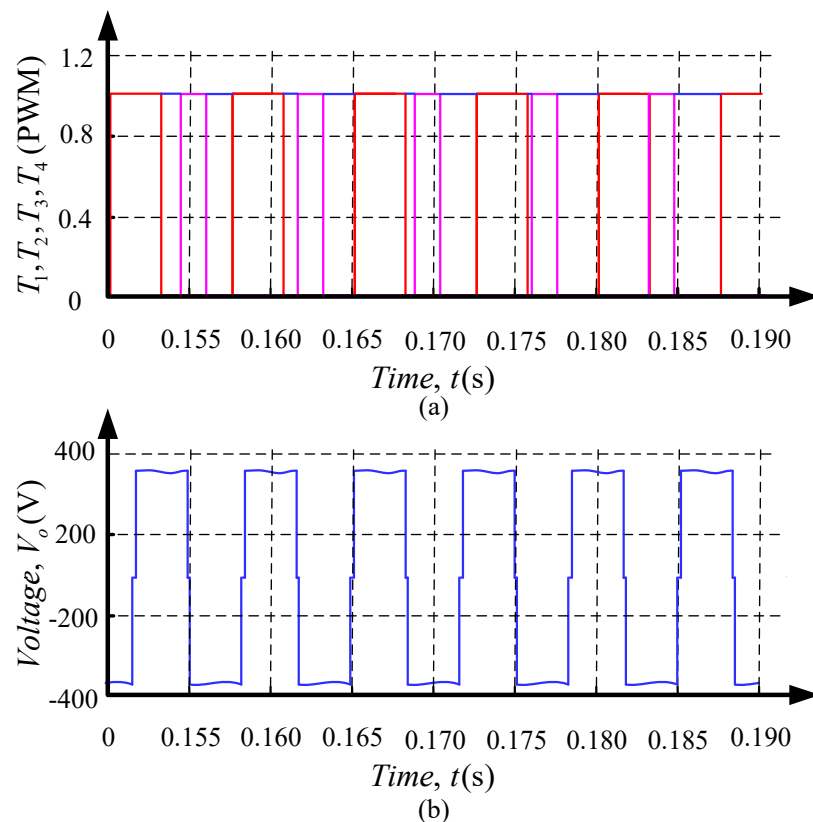


Figure 14. Output: (a) Inverter fuzzy logic PWM; (b) output voltage before filter.

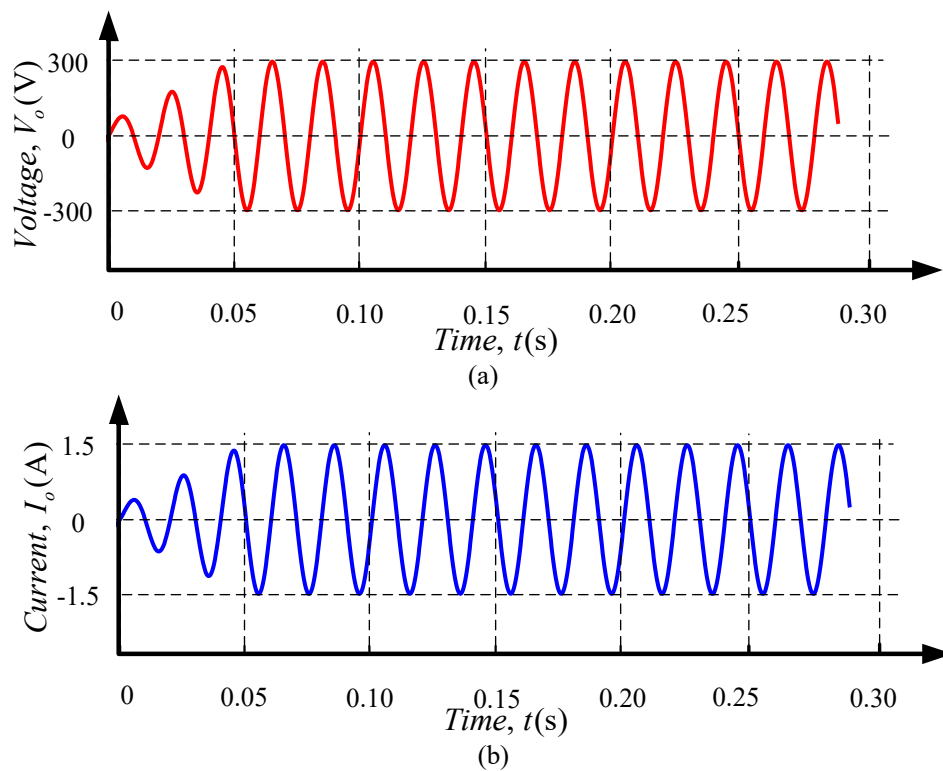


Figure 15. Output: (a) Inverter output voltage; (b) output current.

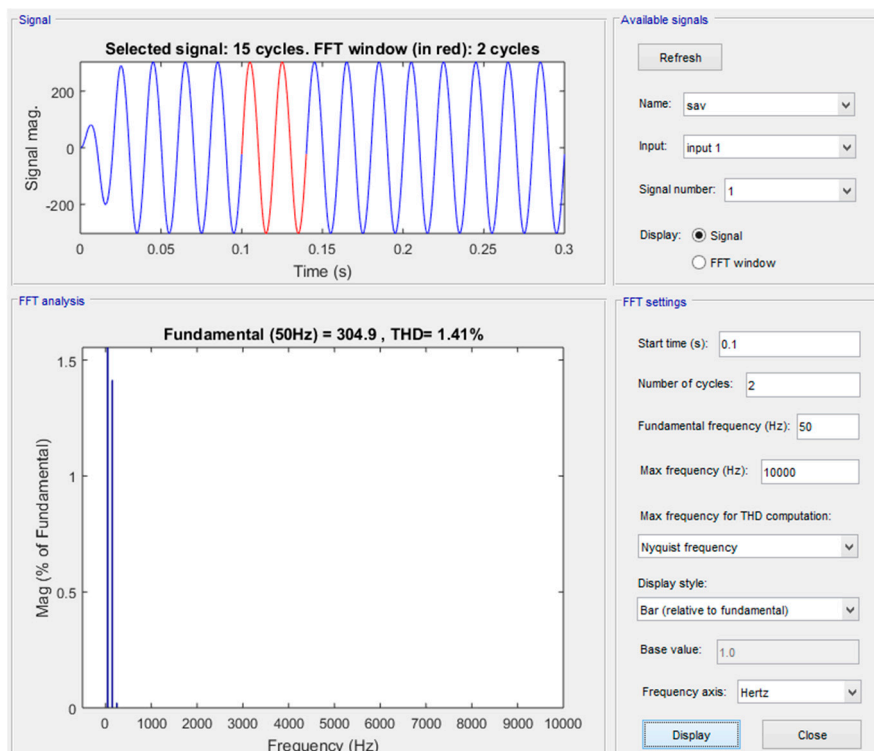


Figure 16. Fast Fourier transform (FFT) analysis of output voltage. THD, total harmonic distortion.

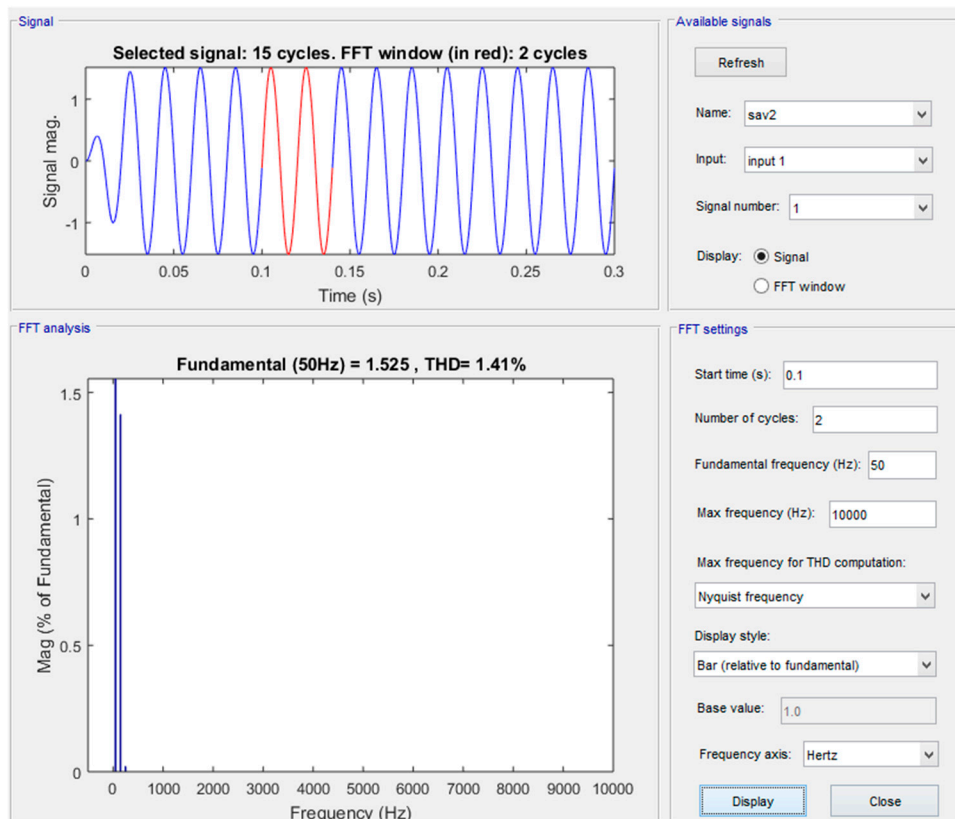


Figure 17. FFT analysis of output current.

Table 5. Tracking time performance comparison [44]. P&O, perturb and observe; INC, incremental conductance.

MPPT Algorithms	Tracking Time of PV Power
P&O	0.300 s
INC	0.250 s
Fuzzy Logic	0.005 s

Comparative Analysis

In this section, a comparative analysis is performed, which is represented in Table 6. The comparative analysis is based on the literature on the fuzzy logic principle. The comparison includes the methodology used with fuzzy logic, implementation complexity, generalization in terms of symmetrical and asymmetrical membership function, inputs to the membership functions, hardware implementation, noise and oscillations near MPP, THD analysis, and the proper filter design. This comparative analysis also distinguishes the proposed research from the previous published literature. As a result, the proposed work has advantages in terms of simple, accurate, and faster convergence to the operating point with minimum noise and THD.

Table 6. Comparative analysis of fuzzy logic based MPPT.

Ref.	Methodology	Implementation	Generalization	Input MFs	Hardware	Noise and Oscillations Near MPP	THD	Proper Filter Design
Proposed	Dual FL based MPPT with PPC	Simple	Sym./Asym. membership	$\Delta P/\Delta I$	×	×	✓	✓
[45]	AFL based MPPT	Simple	Sym./Asym. membership	$\Delta(\Delta P/\Delta I)$	✓	✓	×	×
[46]	FL based MPPT	Complex	Asym. membership	$\frac{\Delta P/\Delta V}{\Delta(\Delta P/\Delta V)}$	✓	✓	×	×
[32]	FL based MPPT with PSO	Complex	Asym. membership	$\Delta P, \Delta V$	✓	✓	×	×
[47]	FL based MPPT	Complex	Sym. membership	$\Delta P, \Delta V$	✓	✓	×	×
[48]	FL based MPPT	Simple	Sym./Asym. membership	$\frac{\Delta P/\Delta t}{\Delta V/\Delta t}$	×	✓	×	×
[49]	FL based MPPT	Simple	Asym. membership	$\frac{\Delta P/\Delta V}{\Delta(\Delta P/\Delta V)}$	✓	✓	×	×
[50]	FL based MPPT	Simple	Sym. membership	$V, \Delta V$	×	✓	×	×
[51]	FL + P&O MPPT	Complex	Sym. membership	$\Delta P, \Delta I$	✓	✓	×	×
[52]	FL + HC MPPT	Complex	Asym. membership	$\frac{\Delta P/\Delta V}{\Delta(\Delta P/\Delta V)}$	✓	✓	×	×
[53]	FL + FO MPPT	Complex	Sym. membership	$\Delta P, \Delta I$	✓	✓	×	×

6. Conclusions

In this paper, an off-grid photovoltaic system with a fuzzy logic MPPT-controlled push pull boost converter is designed. The proposed system is simulated in Matlab/Simulink and tested for various weather conditions. The results proved the efficiency of the fuzzy logic algorithm, which outperforms the conventional algorithms in terms of MPPT accuracy and minimization of fluctuations, regardless of irradiance rapid changes. In addition, the fuzzy logic-based controller designed for the VSI and the adopted LCL filter allow to achieve high performance. The proposed interfacing system between the PV generator and the load is very effective because the provided total harmonic distortion (THD) is 1.41%, which is in agreement with the IEEE standard at the operating frequency.

Author Contributions: Conceptualization, T.-u.H., and F.A.; methodology, F.A.; software, F.A. and K.M.C.; validation, F.A., formal analysis, M.F.T.; investigation, M.F.T.; resources, M.F.T. and K.M.C.; data curation, F.T.; writing—original draft preparation, K.M.; writing—review and editing, K.M., R.A. and H.J.; visualization, I.A.K. and R.M.E.; supervision, T.-u.H.; project administration, T.-u.H.; Funding acquisition, R.A. and H.J. All authors have read and agreed to the published version of the manuscript.

Funding: This research received no external funding.

Conflicts of Interest: The authors declare no conflict of interest.

References

1. Tahir, M.F.; Haoyong, C.; Mehmood, K.; Ali, N.; Bhutto, J.A. Integrated energy system modeling of China for 2020 by incorporating demand response, heat pump and thermal storage. *IEEE Access* **2019**, *7*, 40095–40108. [[CrossRef](#)]
2. Tahir, M.F.; Haoyong, C.; Khan, A.; Javed, M.S.; Laraik, N.A.; Mehmood, K. Optimizing size of variable renewable energy sources by incorporating energy storage and demand response. *IEEE Access* **2019**, *7*, 103115–103126. [[CrossRef](#)]
3. Cheema, K.M. A comprehensive review of virtual synchronous generator. *Int. J. Electr. Power Energy Syst.* **2020**, *120*, 106006. [[CrossRef](#)]
4. Tahmasebi, H. *Boost Integrated High Frequency Isolated Half-Bridge DC-DC Converter: Analysis, Design, Simulation and Experimental Results*; University of Victoria Libraries: Victoria, BC, Canada, 2015.
5. Dolara, A.; Faranda, R.; Leva, S. Energy comparison of seven MPPT techniques for PV systems. *J. Electromagn. Anal. Appl.* **2009**, *2009*, 725. [[CrossRef](#)]
6. Tahir, M.F.; Chen, H.; Javed, M.S.; Jameel, I.; Khan, A.; Adnan, S. Integration of different individual heating scenarios and energy storages into hybrid energy system model of China for 2030. *Energies* **2019**, *12*, 2083. [[CrossRef](#)]

7. Alquthami, T.; Butt, S.E.; Tahir, M.F.; Mehmood, K. Short-term optimal scheduling of hydro-thermal power plants using artificial bee colony algorithm. *Energy Rep.* **2020**, *6*, 984–992.
8. Khan, I.; Li, Z.; Xu, Y.; Gu, W. Distributed control algorithm for optimal reactive power control in power grids. *Int. J. Electr. Power Energy Syst.* **2016**, *83*, 505–513. [[CrossRef](#)]
9. Bhattacharjee, V.; Khan, I. A non-linear convex cost model for economic dispatch in microgrids. *Appl. Energy* **2018**, *222*, 637–648. [[CrossRef](#)]
10. Khan, I.; Xu, Y.; Sun, H.; Bhattacharjee, V. Distributed optimal reactive power control of power systems. *IEEE Access* **2017**, *6*, 7100–7111. [[CrossRef](#)]
11. Khan, I.; Xu, Y.; Kar, S.; Sun, H. Compressive sensing-based optimal reactive power control of a multi-area power system. *IEEE Access* **2017**, *5*, 23576–23588. [[CrossRef](#)]
12. Li, Z.; Mehmood, K.; Zhan, R.; Yang, X.; Qin, Y. Voltage-current double loop control strategy for magnetically controllable reactor based reactive power compensation. In Proceedings of the 2019 IEEE Sustainable Power and Energy Conference (iSPEC), Beijing, China, 20–24 November 2019; pp. 825–830.
13. Mehmood, K.; Hassan, H.T.U.; Raza, A.; Altalbe, A.; Farooq, H. Optimal Power generation in energy-deficient scenarios using bagging ensembles. *IEEE Access* **2019**, *7*, 155917–155929. [[CrossRef](#)]
14. FaizanTahir, M. Optimal load shedding using an ensemble of artificial neural networks. *Int. J. Electr. Comput. Eng. Syst.* **2016**, *7*, 39–46.
15. Muhammad Faizan, T.; Chen, H.; Kashif, M.; Noman Ali, L.; Asad, K.; Muhammad Sufyan, J. Short term load forecasting using bootstrap aggregating based ensemble artificial neural network. *Recent Adv. Electr. Electron. Eng.* **2019**, *12*, 1–11. [[CrossRef](#)]
16. Li, J.; Wang, H. Maximum power point tracking of photovoltaic generation based on the fuzzy control method. In Proceedings of the 2009 International Conference on Sustainable Power Generation and Supply, Nanjing, China, 6–7 April 2009; pp. 1–6.
17. Priyadarshi, N.; Padmanaban, S.; Mihet-Popa, L.; Blaabjerg, F.; Azam, F. Maximum power point tracking for brushless DC motor-driven photovoltaic pumping systems using a hybrid ANFIS-FLOWER pollination optimization algorithm. *Energies* **2018**, *11*, 1067. [[CrossRef](#)]
18. Kebir, T.; Filiz, G.; Larbes, C.; Ilinca, A.; Obeidi, T.; Tchoketch Kebir, S. Study of the intelligent behavior of a maximum photovoltaic energy tracking fuzzy controller. *Energies* **2018**, *11*, 3263. [[CrossRef](#)]
19. Priyadarshi, N.; Ramachandaramurthy, V.K.; Padmanaban, S.; Azam, F. An ant colony optimized MPPT for standalone hybrid PV-wind power system with single Cuk converter. *Energies* **2019**, *12*, 167. [[CrossRef](#)]
20. Wang, Y.; Yang, Y.; Fang, G.; Zhang, B.; Wen, H.; Tang, H.; Fu, L.; Chen, X. An advanced maximum power point tracking method for photovoltaic systems by using variable universe fuzzy logic control considering temperature variability. *Electronics* **2018**, *7*, 355. [[CrossRef](#)]
21. Ma, S.; Chen, M.; Wu, J.; Huo, W.; Huang, L. Augmented nonlinear controller for maximum power-point tracking with artificial neural network in grid-connected photovoltaic systems. *Energies* **2016**, *9*, 1005. [[CrossRef](#)]
22. Li, C.; Chen, Y.; Zhou, D.; Liu, J.; Zeng, J. A high-performance adaptive incremental conductance MPPT algorithm for photovoltaic systems. *Energies* **2016**, *9*, 288. [[CrossRef](#)]
23. Piegari, L.; Rizzo, R.; Spina, I.; Tricoli, P. Optimized adaptive perturb and observe maximum power point tracking control for photovoltaic generation. *Energies* **2015**, *8*, 3418–3436. [[CrossRef](#)]
24. Cheema, K.M.; Mehmood, K. Improved virtual synchronous generator control to analyse and enhance the transient stability of microgrid. *IET Renew. Power Gener.* **2020**, *14*, 495–505. [[CrossRef](#)]
25. Yau, H.-T.; Wu, C.-H. Comparison of extremum-seeking control techniques for maximum power point tracking in photovoltaic systems. *Energies* **2011**, *4*, 2180–2195. [[CrossRef](#)]
26. Salas, V.; Olias, E.; Barrado, A.; Lazaro, A. Review of the maximum power point tracking algorithms for stand-alone photovoltaic systems. *Sol. Energy Mater. Sol. Cells* **2006**, *90*, 1555–1578. [[CrossRef](#)]
27. Srdovic, M.; Familant, Y.L.; Grandi, G.; Ruderman, A. Time-domain minimization of voltage and current total harmonic distortion for a single-phase multilevel inverter with a staircase modulation. *Energies* **2016**, *9*, 815. [[CrossRef](#)]
28. Dolara, A.; Leva, S. Power quality and harmonic analysis of end user devices. *Energies* **2012**, *5*, 5453–5466. [[CrossRef](#)]
29. Trubitsyn, A. *High Efficiency DC/AC Power Converter for Photovoltaic Applications*; Massachusetts Institute of Technology: Cambridge, MA, USA, 2010.

30. Sharaf, F.Y. Designing Power Inverter with Minimum Harmonic Distortion Using Fuzzy Logic Control. 2014. Available online: <https://195.189.210.17/handle/20.500.12358/18855> (accessed on 15 June 2020).
31. Li, J.; Wang, H. A novel stand-alone PV generation system based on variable step size INC MPPT and SVPWM control. In Proceedings of the 2009 IEEE 6th International Power Electronics and Motion Control Conference, Wuhan, China, 17–20 May 2009; pp. 2155–2160.
32. Cheng, P.-C.; Peng, B.-R.; Liu, Y.-H.; Cheng, Y.-S.; Huang, J.-W. Optimization of a fuzzy-logic-control-based MPPT algorithm using the particle swarm optimization technique. *Energies* **2015**, *8*, 5338–5360. [[CrossRef](#)]
33. Maiti, D.; Mondal, N.; Biswas, S. *Design Procedure of a Push Pull Current-Fed DC-DC Converter*; Jadavpur University: Kolkata, India, 2010.
34. Blooming, T.M.; Carnovale, D.J. Application of IEEE Std 519-1992 harmonic limits. In Proceedings of the Conference Record of 2006 Annual Pulp and Paper Industry Technical Conference, Appleton, WI, USA, 18–22 June 2006; pp. 1–9.
35. Adhikari, N.; Singh, B.; Vyas, A.L.; Chandra, A. Analysis and design of isolated solar-PV energy generating system. In Proceedings of the 2011 IEEE Industry Applications Society Annual Meeting, Orlando, FL, USA, 9–13 October 2011; pp. 1–6.
36. Singh, S.; Mathew, L.; Shimi, S. Design and simulation of intelligent control MPPT technique for PV module using MATLAB/SIMSCAPE. *Int. J. Adv. Res. Electr. Electron. Instrum. Eng.* **2013**, *2*, 4554–4566.
37. Wang, C. A Study of Membership Functions on Mamdani-Type Fuzzy Inference System for Industrial Decision-Making. Master's Thesis, Lehigh University, Bethlehem, PA, USA, 2015.
38. Usta, M.A.; Akyazi, Ö.; Altaş, İ.H. Design and performance of solar tracking system with fuzzy logic controller used different membership functions. In Proceedings of the 2011 7th International Conference on Electrical and Electronics Engineering (ELECO), Bursa, Turkey, 1–4 December 2011; pp. II-381–II-385.
39. Mudi, R.K.; Pal, N.R. A robust self-tuning scheme for PI-and PD-type fuzzy controllers. *IEEE Trans. Fuzzy Syst.* **1999**, *7*, 2–16. [[CrossRef](#)]
40. Shehata, A.; Metered, H.; Oraby, W.A. Vibration control of active vehicle suspension system using fuzzy logic controller. In *Vibration Engineering and Technology of Machinery*; Springer: Berlin/Heidelberg, Germany, 2015; pp. 389–399.
41. Reznik, A.; Simões, M.G.; Al-Durra, A.; Muyeen, S. LCL filter design and performance analysis for grid-interconnected systems. *IEEE Trans. Ind. Appl.* **2013**, *50*, 1225–1232. [[CrossRef](#)]
42. Mendel, J.M. Fuzzy logic systems for engineering: A tutorial. *Proc. IEEE* **1995**, *83*, 345–377. [[CrossRef](#)]
43. Kahlane, A.; Hassaine, L.; Kherchi, M. LCL filter design for photovoltaic grid connected systems. *J. Renew. Energies* **2014**, *2014*, 227–232.
44. Suwannatrain, P.; Liutanakul, P.; Wipasuramont, P. Maximum power point tracking by incremental conductance method for photovoltaic systems with phase shifted full-bridge dc-dc converter. In Proceedings of the 8th Electrical Engineering/Electronics, Computer, Telecommunications and Information Technology (ECTI) Association of Thailand-Conference 2011, Khon Kaen, Thailand, 17–19 May 2011; pp. 637–640.
45. Rezk, H.; Aly, M.; Al-Dhaifallah, M.; Shoyama, M. Design and hardware implementation of new adaptive fuzzy logic-based MPPT control method for photovoltaic applications. *IEEE Access* **2019**, *7*, 106427–106438. [[CrossRef](#)]
46. Liu, C.-L.; Chen, J.-H.; Liu, Y.-H.; Yang, Z.-Z. An asymmetrical fuzzy-logic-control-based MPPT algorithm for photovoltaic systems. *Energies* **2014**, *7*, 2177–2193. [[CrossRef](#)]
47. Ozdemir, S.; Altin, N.; Sefa, I. Fuzzy logic based MPPT controller for high conversion ratio quadratic boost converter. *Int. J. Hydrogen Energy* **2017**, *42*, 17748–17759. [[CrossRef](#)]
48. Robles Algarín, C.; Taborda Giraldo, J.; Rodríguez Álvarez, O. Fuzzy logic based MPPT controller for a PV system. *Energies* **2017**, *10*, 2036. [[CrossRef](#)]
49. El Khateb, A.; Abd Rahim, N.; Selvaraj, J.; Uddin, M.N. Fuzzy-logic-controller-based SEPIC converter for maximum power point tracking. *IEEE Trans. Ind. Appl.* **2014**, *50*, 2349–2358. [[CrossRef](#)]
50. Kottas, T.L.; Boutalis, Y.S.; Karlis, A.D. New maximum power point tracker for PV arrays using fuzzy controller in close cooperation with fuzzy cognitive networks. *IEEE Trans. Energy Convers.* **2006**, *21*, 793–803. [[CrossRef](#)]
51. Zainuri, M.A.A.M.; Radzi, M.A.M.; Soh, A.C.; Abd Rahim, N. Development of adaptive perturb and observe-fuzzy control maximum power point tracking for photovoltaic boost dc-dc converter. *IET Renew. Power Gener.* **2013**, *8*, 183–194. [[CrossRef](#)]

52. Alajmi, B.N.; Ahmed, K.H.; Finney, S.J.; Williams, B.W. Fuzzy-logic-control approach of a modified hill-climbing method for maximum power point in microgrid standalone photovoltaic system. *IEEE Trans. Power Electron.* **2010**, *26*, 1022–1030. [[CrossRef](#)]
53. Tang, S.; Sun, Y.; Chen, Y.; Zhao, Y.; Yang, Y.; Szeto, W. An enhanced MPPT method combining fractional-order and fuzzy logic control. *IEEE J. Photovolt.* **2017**, *7*, 640–650. [[CrossRef](#)]



© 2020 by the authors. Licensee MDPI, Basel, Switzerland. This article is an open access article distributed under the terms and conditions of the Creative Commons Attribution (CC BY) license (<http://creativecommons.org/licenses/by/4.0/>).